Spectral analysis of energy transfer in variable density, radiatively heated particle-laden flows

By H. Pouransari, H. Kolla†, J. H. Chen† AND A. Mani

We investigate the influence of radiative heating of particles on the turbulence energy spectra of the background carrier fluid. Radiative heating of particles and ensuing heat transfer to the fluid introduces dilatation, which considerably influences the turbulence cascade of the gas phase. Turbulent kinetic energy is introduced at high wave numbers via the pressure-dilatation term that results in an increasing amount of kinetic energy shifting to the divergence modes of velocity compared with that founds in the divergence-free modes. The wave number range over which this occurs also broadens over time. The spectral energy transfer term is also affected by radiation with the crossover from positive to negative values of this term moving to higher wave numbers with increasing radiation.

1. Introduction

Particle-laden turbulent flows occur in many scenarios such as cloud formation, urban pollutant dispersion, multi-phase flows, and solid fuel combustion. In the simplest case the particles are passive and are purely advected by the flow with no feedback from the particles to the carrier fluid phase. Tracer-based measurement techniques such as particle image velocimetry (PIV) rely on such an assumption. However, in most cases there is a complex two-way coupling where mass, momentum, and energy of both the particles and fluid phase are affected by each other. This is even more complicated if the fluid phase is turbulent since the particles can fundamentally disrupt the multi-scale turbulence cascade. This makes the study of particle-laden turbulent flows challenging, yet relevant.

The specific focus in this study is on a particle-laden solar receiver application. This application comprises solid particles dispersed in background fluid medium that is thermally heated by solar radiation. The heat is transferred to the fluid phase, which is recovered downstream and can be used, for example, for power generation or chemical conversion. The optimal design of such a receiver requires a good understanding of the coupling between the heating of the particles and the dynamics of the carrier fluid. In particular we ask the question: is the carrier fluid turbulence affected by particle heating? Even in the absence of radiative heating there is a range of well-studied phenomena that result from by the particle interaction with the turbulent eddies such as preferential concentration of particles in regions of low vorticity (Squires & Eaton 1991), preferential sweeping of particles with high inertia in cases where gravity is present (Wang & Maxey 1993), and fluid acceleration by particle drag at high particle concentrations that in turn enhances particle settling velocity (Bosse *et al.* 2006).

Conceivably, particle heating by radiation will introduce additional coupling phenomena because the heat transfer from the particles will cause fluid dilatation and velocity

† Combustion Research Facility, Sandia National Laboratories

fluctuations at corresponding scales. In an analogous setting turbulent combustion flame-induced fluid dilatation was observed to affect the turbulence kinetic energy spectrum at wave numbers corresponding to the flame scales. We are interested in investigating whether similar phenomenon arises in radiatively heated particle flows. We employ direct numerical simulations to study the kinetic energy spectra of homogeneous isotropic turbulent flows with radiatively heated particles. We compare the energy spectra with those of identical turbulent flows that do not have particle heating by radiation. To focus purely on the heating effect we consider a regime where the point-particle assumption is valid and particle collisions do not occur. We also ignore effects of gravity. We pay special attention to the role of dilatation and its influence on the cascade and energy transfer across scales. The rest of the paper is organized as follows. Section 2 presents a brief overview of the mathematical framework used to study the kinetic energy spectra. The details of the direct numerical simulations, methodology, and relevant parameters investigated are presented in Section 3. The results are presented in Section 4.

2. Mathematical framework

A novel aspect of this study is the use of a variable-density formulation to study kinetic energy spectra, the details of which are presented here. Both in turbulent combustion and in the present application the mechanism by which the turbulent flow is affected by density change at the fine scales is of an order comparable to or smaller than the Kolmogorov scale. The traditional mathematical framework for studying spectra and energy dynamics in spectral space is valid for constant density flows and cannot be applied in a straightforward fashion to variable density flows. Kolla *et al.* (2014) proposed a density-weighted formulation for two-point velocity correlation tensors that allows the study of energy spectra in variable density flows. The formulation, based on conservation laws for variable density flows, yields a balance equation for Favre averaged turbulence kinetic energy in wave number space. The balance equation illuminates the role of various quantites such as pressure fluctuation, dilatation, mean velocity gradient, density fluctuation, and dissipation on the kinetic energy balance in wave number space.

The framework is centered on the following definition for two-point velocity correlation tensor

$$\widetilde{R}_{ij}(\vec{\mathrm{r}}) = \frac{1}{2\overline{\rho}}\Big[\ \overline{\rho u_i(\vec{\mathrm{x}})\ u_j(\vec{\mathrm{x}}+\vec{\mathrm{r}})}\quad +\quad \overline{u_i(\vec{\mathrm{x}})\ \rho u_j(\vec{\mathrm{x}}+\vec{\mathrm{r}})}\ \Big], \tag{2.1}$$

where ρ is density and u_i denotes the i^{th} component of velocity fluctuation. The overline denotes an averaging over the position vector $\vec{\mathrm{x}}$ in homogeneous directions, whereas the vector $\vec{\mathrm{r}}$ denotes the separation vector. Note that upon contracting the tensorial indices and setting the separation vector to zero, the two-point correlation tensor yields the Favre-averaged turbulent kinetic energy, analogous to its constant density counterpart. Using this property and starting from conservation equations for ρu_i and u_i in variable density flows, a balance equation for Favre-averaged turbulent kinetic energy in wave number space was derived and presented in Kolla *et al.* (2014).

The derivation is not presented in detail here, and the reader is referred to the original paper, but we focus on the two key terms that are relevant for the present application. For the homogeneous isotropic configuration chosen in the present study there are no gradients of mean quantities. This reduces the relevant terms in the energy spectra balance equation to only three (Kolla *et al.* 2014): a pressure-dilatation term that represents a source, a density-weighted triple velocity correlation term that transfers energy across

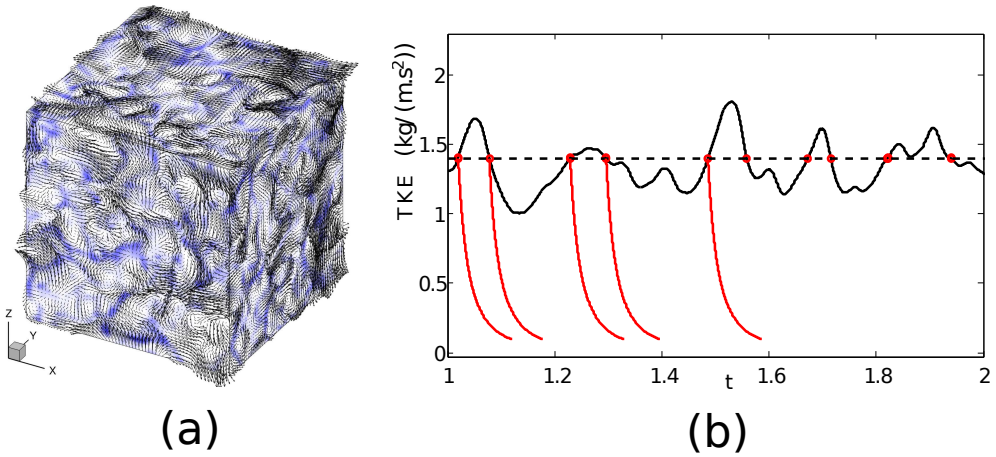

FIGURE 1. Computational domain, projected gas velocity vectors, and contours of particles concentration (a), Averaged turbulent kinetic energy per unit volume (kg/(m.s^2)) as a function of time (s) in a forced homogeneous isotropic turbulence (b).

wave numbers, and a molecular dissipation term. Here, in addition to the energy spectra themselves, we focus on the first two terms:

The pressure-dilatation term encapsulates the effect of fluid dilatation owing to particle heating. This term is of the form

$$\frac{1}{\overline{\rho}}\left[\overline{\mathcal{F}\{p\}\mathcal{F}^*\{\frac{\partial u_j}{\partial x_j}\}} + \overline{\mathcal{F}\{\rho u_j\}\mathcal{F}^*\{\frac{1}{\rho}\frac{\partial p}{\partial x_j}\}}\right], \tag{2.2}$$

where $\mathcal{F}$ denotes the Fourier transform operator and $\mathcal{F}^*$ its complex conjugate.

The density-weighted triple velocity correlation term represents energy transfer between wave numbers because its integral over all wave numbers is identically zero. This term is of the form

$$\frac{1}{\overline{\rho}}\left[\overline{\mathcal{F}^*\{\rho u_j\}\mathcal{F}\{u_k\frac{\partial u_j}{\partial x_k}\}} + \overline{\mathcal{F}^*\{u_j\}\mathcal{F}\{\frac{\partial \rho u_j u_k}{\partial x_k}\}}\right]. \tag{2.3}$$

While the pressure dilatation term is interesting to study because it denotes the primary role of density change by dilatation, the energy transfer term is interesting because it quantifies any backscatter that might arise from the energy being injected at high wave numbers by the pressure-dilatation term.

3. DNS details

Direct numerical simulations of decaying homogeneous isotropic turbulence laden with particles in a periodic box were performed using an Eulerian-Lagrangian high fidelity code. Figure 1(a) illustrates a snapshot of the DNS domain. Gas solution points are located on a structured uniform staggered grid, whereas particles are treated as Lagrangian points moving around the domain. These calculations are second-order accurate in space, and fourth-order accurate in time for both the gas and dispersed phases.

To generate appropriate initial conditions for our physical analysis, each simulation begins with an initial turbulent field similar to Kwak *et al.* (1975), and random uniform distribution of particles but with no radiative heating. Turbulence is sustained using

artificial linear forcing as explained in Rosales & Meneveau (2005), and the simulation is performed until the turbulence develops fully and the spatial distribution of the particles becomes statistically stationary. After the particle-laden turbulence fully develops, we start identifying snapshots in time when the total turbulent kinetic energy is equal to the nominal mean value. In Figure 1(b) the evolution of turbulent kinetic energy as a function of time is plotted during the forcing period. The circles correspond to instances when the TKE of the instantaneous field is equal to the mean TKE. Each one of these snapshots is used as the initial condition for a target calculation in which turbulence decays and radiation is present, and these snapshots are selected to be separated by a time much greater than the large-eddy turn over time so that the resulting calculations may be deemed statistically independent. During the target calculations themselves the turbulence is no longer forced and decays, while the target thermal radiation to the particles is switched on. For improved convergence we used multiple realizations for each case to obtain averaged statistics. Each red curve in Figure 1(b) corresponds to one such realization.

The inhomogeneous heat transfer from hot particles to the gas brings about variation in the density field. The flow conditions correspond to the low-Mach number regime and therefore the hydrodynamic pressure is much smaller than the thermodynamic pressure. This allows us to consider a constant thermodynamic pressure in space, which is governed by the ideal gas law. Because of the heat transfer to the system, thermodynamic pressure can increase with time; however, in this study the temporal variation of thermodynamic pressure is negligible. Variation in the gas density field results in a variable coefficient Poisson equation for the hydrodynamic pressure. The Poisson equation is solved using an iterative spectral method. Zamansky *et al.* (2014) showed that a particle-laden turbulence subjected to external radiation and gravity produces a sustained turbulence. Here, similar to analogous regimes in combustion, we ignore the effect of gravity justified by considering small domains and fast processes (large Froude number) and focus solely on the effects of heating on fluid dilatation.

The set of parameters used in this study are listed in Table 1. Using a 256^3 grid for the gas phase, the initial (at the beginning of decay) turbulence Reynolds number based on Taylor's micro scale is $\mathrm{Re}_\lambda = 67$. The corresponding Kolmogorov length and time scales are 1.06×10^{-4} m and 7×10^{-4} s, and the grid spacing and time step of the DNS are 1.56×10^{-4} m and 5×10^{-5} s, respectively. Physical properties of the particle (particle mass, heat capacity etc.) are assumed to be those of Nickel and the particle diameter is much smaller than the Kolmogorov length scale; hence, the point particle assumption is valid. In order to track particles we have used the Maxey & Riley (1983) equation. In this case, only the Stokes drag term is significant. The initial Stokes number (the ratio of particle relaxation time to the Kolmogorov time scale) is 5.3. Moreover, we have neglected the momentum two-way coupling between gas and particles in order to study, in isolation, the effect of particle-to-gas heat transfer. The nominal mass loading ratio in this study is 13%. At such a significant Stokes number and mass loading the momentum one-way coupling may not be a safe assumption. However, as noted earlier, our focus is to study the effects of thermal radiation in isolation.

The radiation is modeled using an optically thin assumption. This means that the external radiation is uniformly available to all particles, and particle-to-particle radiation scattering is negligible. Therefore, particles absorb thermal radiation and transfer thermal energy to their surrounding gas by conduction. We have considered four different cases to study the turbulence evolution: (i) no radiation, (ii) nominal radiation with particle

parameter	description	value	parameter	description	value
Re_λ	initial Reynolds	67	W	box size	4 cm
ρ_0	gas initial density	1.2 kg/m^3	κ	mass load ratio	13%
T_0	initial temperature	300 K	μ_0	gas viscosity	0.019 mPa.s
C_p	gas heat cap.	1012 J/(kg.K)	C_v	gas heat cap.	723 J/(kg.K)
C_{vp}	particle heat cap.	450 J/(kg.K)	n_0	particle # dens.	$2{\cdot}10^{10}$ m^{-3}
D_p	particle diameter	12 μm	ρ_p	particle density	8900 kg/m^3
ϵ_p	emissivity	0.4	I_0	rad. intensity	4.69 MW/m^2

TABLE 1. Nominal parameters used in this study

number density $n_0 = 2 \cdot 10^{10}$ m^{-3}, (iii) nominal radiation with particle number density $n_0 = 8 \cdot 10^{10}$ m^{-3}, (iv) nominal radiation with particle number density $n_0 = 3.2 \cdot 10^{11}$ m^{-3}.

Note that all parameters except the particle number density are the same among different cases. Higher particle number density results in a higher total radiation absorption. For each case, five different realizations are simulated. For each realization data is collected at an interval of 0.01 s, which is approximately equal to one large eddy turn over time.

4. Results

In this section, various results of different cases are presented. Results for each case are averaged over 5 independent realizations. The one dimensional turbulent kinetic energy spectrum for a variable density flow is obtained as follows

$$E_k = \frac{1}{2} \iint \sum_{j=1}^{3} \left(\widehat{\rho u}_j^* \hat{u}_j + \widehat{\rho u}_j \hat{u}_j^* \right). \tag{4.1}$$

In the above equation the hat operator, $\widehat{..}$, denotes the three-dimensional Fourier transform, and operator * denotes its complex conjugate. The double integral is taken over a spherical shell in wave space.

As mentioned in section 3 the gas phase solution points are stored on a uniform staggered grid, i.e., the gas momentum in each direction is stored on cell faces, and gas density and hydrodynamic pressure are stored at each cell center. In order to compute the energy spectrum using Eq-(4.1), we need to compute the gas momentum and velocity in all directions at the cell center. This requires a couple of interpolations. In the following, the process to interpolate the gas velocity field from the cell faces to cell centers is explained: (i) interpolate density from cell centers to cell faces using linear interpolation, (ii) compute velocity at cell faces $u_j = (\rho u)_j / \rho_{\mathrm{face}_j}$, (iii) take 3D Fourier transform of each velocity component: $\hat{u}_j = \mathcal{F}(u_j)$, (iv) shift $\hat{u}_j$ by half a grid size: $\hat{u}_j^{\mathrm{shifted}} = \exp(-i\Delta x_j/2).\hat{u}_j$, (v) take the inverse Fourier transform of $\hat{u}_j^{\mathrm{shifted}}$ to obtain u_j at cell centers.

Note that the momentum interpolation is similar, except that the first two steps are not required. The advantage of the above interpolation scheme is that the divergence-free condition of the flow is preserved. Essentially, if the flow is incompressible with constant density, then the divergence of the gas momentum (which in this case is a constant factor of the velocity) is zero at cell centers. This means that the Fourier transform of velocity

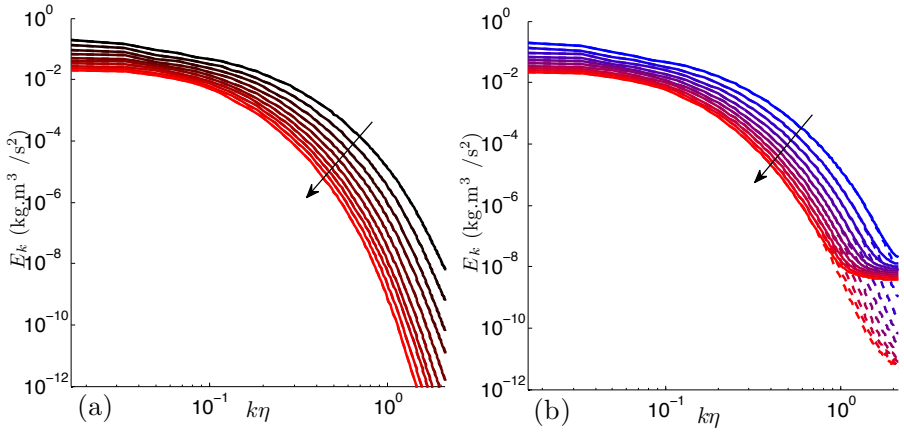

FIGURE 2. Turbulent kinetic energy spectra (kg.m^3/s^2) for decaying homogeneous isotropic turbulence at every large-eddy turn over time: no radiation (a), with radiation (b). The arrow shows the direction in time. The solid line is the total turbulent kinetic energy. The dashed line is the contribution of the divergence-free part of the velocity in the total turbulent kinetic energy.

is perpendicular to the modified wave number vector. Note that here we are using a central difference to calculate the divergence. Because in the above interpolation scheme the Fourier transform of the velocity is unchanged (it is only shifted), the orthogonality condition will be preserved. For a general flow, with variable density, the above scheme does not produce artificial divergence.

4.1. *Energy spectra with radiative heating*

In the absence of a source, homogeneous isotropic turbulence decays in time. In Figure 2(a) the turbulent kinetic energy spectra for a decaying homogeneous isotropic turbulence is plotted for ten large eddy turnover times. The large eddy turnover time is defined using the initial values of the integral length scale and u_{rms}. Turbulence attenuation takes place at all wave numbers. Figure 2(b) shows the evolution of turbulent kinetic energy spectra in decaying homogeneous isotropic turbulence, when external radiation is turned on. Particle-turbulence interaction results in preferential concentration of particles (Eaton & Fessler 1994). Hence, radiatively heated particles transfer energy to the gas phase inhomogeneously. This strengthens the turbulence at all wave-numbers, but more significantly at higher wave numbers. Essentially, while the overall turbulence decays, radiation results in accumulation of energy at high wave-numbers. This results in plateaus in the energy spectra at high wave number dissipative range as shown in the Figure 2(b) (solid lines). Interestingly, the strength of the plateau increases as time progresses, reflecting an accumulation of energy at high wave numbers over time. An identical behaviour was observed in turbulent combustion (Kolla *et al.* 2014) where the energy spectrum displayed a plateau at high wave numbers corresponding to dilatation generated at the flame scales.

As conjectured earlier, the physical mechanism for introduction of turbulent fluctuations at high wave numbers through flow dilatation is responsible for the plateau in energy spectra. In order to understand the turbulence modification caused by heat transfer from point particles, we investigate the modification of the divergence-free modes of the flow separately. This is accomplished by decomposing the gas momentum and velocity as

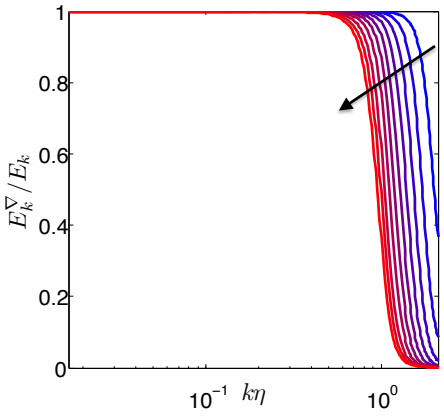

FIGURE 3. Shown is the fraction of turbulent kinetic energy owing divergence-free modes as a function of non-dimensionalized wave number for a decaying particle-laden homogeneous isotropic turbulence subject to radiation. Different curves correspond to snapshots at every large-eddy turnover time. The arrow shows the direction in time.

follows

$$u_i = u_i^\nabla + u_i' \quad , \quad \rho u_i = \rho u_i^\nabla + \rho u_i' \; . \tag{4.2}$$

The superscript ∇ denotes the divergence free part of a field (i.e., a Helmholtz-Leray decomposition). Accordingly, we can define the turbulence kinetic energy spectrum due to the divergence-free modes as follows:

$$E_k^\nabla = \frac{1}{2} \iint \sum_{j=1}^{3} \left(\widehat{\rho u_j^\nabla}^* \widehat{u_j^\nabla} + \widehat{\rho u_j^\nabla} \widehat{u_j^\nabla}^* \right) \; . \tag{4.3}$$

In Figure 2 dashed lines show E_k^∇ at different times. In the case with no radiation (Figure 2(a)) the energy in the divergence-free modes is equal to the total energy and hence the solid and dashed lines are coincident. However, with radiative heating, the contribution of the divergence-free modes decreases at higher wave-numbers as evident in the right plot. In other words, the particle-to-gas heat transfer modifies the divergence modes of the flow more significantly. In Figure 3 the ratio of turbulent kinetic energy of the divergence-free modes to the total energy is plotted as a function of wave number at different times. These Z-shaped curves shift toward the left along the x-axis as time progresses indicating that while energy is increasingly accumulating in the divergence modes, the wave number range over which this occurs also keeps broadening.

Note that as time progresses, three different phenomena take place simultaneously: turbulence decays, more radiation is absorbed, and Stokes number decreases. Stokes number is the ratio of the particle relaxation time and the Kolmogorov time scale. As time progresses turbulence decays, therefore, Kolmogorov time scale increases. This results in smaller Stokes number. The initial Stokes number is St = 5.3. Therefore, as time progresses, Stokes number approaches unity and stronger clusters of particles form (Eaton & Fessler 1994).

To study the effect of radiation, we have considered three different cases in terms of the total radiation absorption by the system. One way to increase the total radiation absorption is by increasing the number of particles. Because the mixture is assumed to be optically thin, increasing the number of particles results in a proportionate increase in

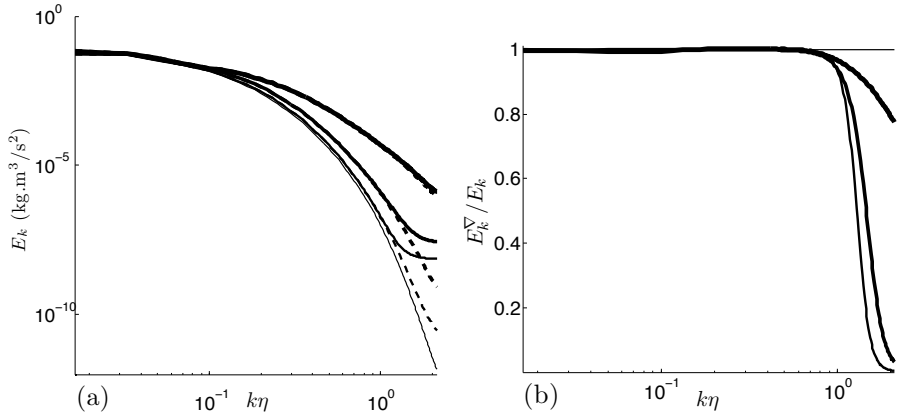

FIGURE 4. Turbulence kinetic energy spectra (kg.m^3/s^2) in a decaying particle-laden homogeneous isotropic turbulence subject to radiation, after 5 large-eddy turnover times. Four cases: no radiation, nominal radiation, nominal radiation $\times 4$, and nominal radiation $\times 16$. Thicker lines correspond to more radiation cases. The dashed lines are the divergence-free contribution (a). The fraction of turbulent kinetic energy from divergence-free modes (b).

the total radiation energy absorption. The nominal particle number density is $n_0 = 2{\cdot}10^{10}$ m^{-3}. We have considered cases with 4 and 16 times more particles as well. An alternative way to increase the total radiation absorption is to increase the radiation intensity while holding the particle number density fixed. We compared a case with 16 times higher radiation intensity and find that the results are identical to the case with 16 times higher particle density, and hence only show results with varying particle density. In Figure 4 the results of various radiation cases are compared with the no radiation case. The left plot suggests that higher total radiation modifies the energy spectrum more significantly, and over a wider range of wave numbers. The right plot suggests that in cases with higher radiation, the contribution of the divergence-free mode is greater. In effect, by increasing the total radiation, the impact of heat transfer on turbulence shifts from affecting only the divergence modes to affecting both the divergence and divergence-free modes.

4.2. *Influence of dilatation*

It is evident from Figures 3 and 4 that dilatation plays a central role in the modification of the energy spectra. As noted in section 2 the role of dilatation in the balance equation for the energy spectrum is encapsulated in the pressure-dilatation term. We have evaluated the pressure-dilatation term as in Eq. (2.2) and these are presented for selected instants for all cases in Figure 5. The plots clearly show that the pressure-dilatation term changes sign from negative to positive and acts as a source at high wave numbers when radiative heating is active. This change in behavior occurs at wave numbers that precede the wave numbers corresponding to the plateau in the energy spectra in Figure 4. Note that the y axis in Figure 4 is on a logarithmic scale, whereas in Figure 5 it is on a linear scale. The strength of the dilatation influence depends on the radiation level and an absence of this effect is apparent for the case with no radiation. Furthermore, the right plot in Figure 5 shows that as time progresses the magnitude of the pressure-dilatation term decreases for all cases, consistent with the plots in Figure 4. This suggests that, possibly, the energy shifts from the dilatational modes to the divergence-free modes as time progresses and this occurs faster for the higher radiation cases.

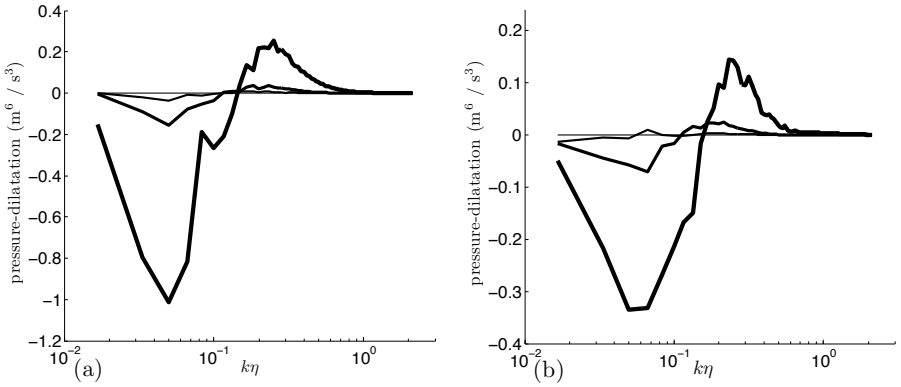

FIGURE 5. Pressure-dilatation term as in Eq. (2.2) (m^6/s^3) for four cases at two instants: 1-eddy turnover time (a), and 5-eddy turnover times (b). The cases are distinguished by the line thickness with the thinnest line corresponding to the no radiation case and the thickest line corresponding to the highest radiation case.

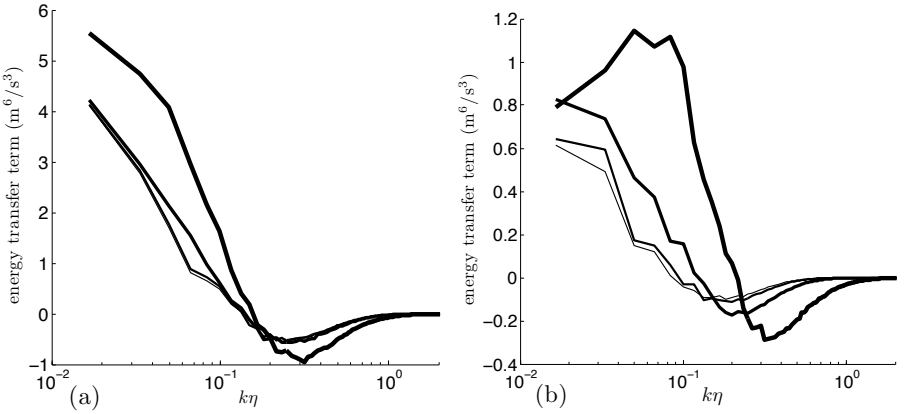

FIGURE 6. Energy transfer term as in Eq. (2.3) (m^6/s^3) plotted on a linear-log axes for the four cases at two instants: 1-eddy turn over time (a) and 5-eddy turn over times (b). Thickness of lines is used to distinguish the cases as in Figure 5.

4.3. *Spectral energy transfer*

Since the mechanism of turbulent energy injection at high wave numbers is evident through the dilatation influence, it is interesting to study the energy transfer across wave numbers. Typically, one would expect the energy transfer to be unidirectional (from low to high wave numbers) if the conventional cascade applies. However, it is clear that the cascade is disrupted at the high wave number dissipative range. The energy balance is liable to be disrupted by this. This will have consequences, particularly from an LES modeling point of view, if the net energy transfer reverses at any of the wave numbers. With this motivation, we compute the energy transfer term as in Eq. (2.3), and its evolution in time, and these are shown in Figure 6. It is evident that even at early instant of 1 turn over time the transfer term is affected by radiation with the crossover from positive to negative values shifting to higher wave numbers with increasing radiation. This trend is even more pronounced at the later instant of 5 eddy turnover times, indicating that the cumulative effects of radiative heating disrupt the energy transfer.

5. Conclusions

The influence of radiative heating of particles, and ensuing heat transfer, on the energy cascade of particle laden turbulent flows seems analogous to that of heat release in turbulent flames. Heating of the particles imparts dilatation to the carrier fluid, which introduces energy into the divergence modes in a flow that is otherwise divergence-free. The energy in the divergence modes appears at high wave numbers where dilatation is most active, and this wave number range broadens with time, denoting a cumulative effect over time. Increasing the total radiation absorption seems to result in both the divergence and divergence-free modes being affected. Both the pressure-dilatation term, which encapsulates the high wave number dilatation source to turbulent kinetic energy, and the energy transfer term increase in magnitude with increase in total radiation.

Acknowledgments

The authors acknowledge use of computational resources from the Certainty cluster awarded by the National Science Foundation to CTR.

REFERENCES

Bosse, T., Kleiser, L. & Meiburg, E. 2006 Small particles in homogeneous turbulence: Settling velocity enhancement by two-way coupling. *Phys. Fluids* **18**, 027102.

Eaton, J. K. & Fessler, J. 1994 Preferential concentration of particles by turbulence. *Int. J. Multiphase Flow* **20**, 169–209.

Kolla, H., Hawkes, E. R., Kerstein, A. R., Swaminathan, N. & Chen, J. H. 2014 On velocity and reactive scalar spectra in turbulent premixed flames. *J. Fluid Mech* **754**, 456–487.

Kwak, D., Reynolds, W. & Ferziger, J. 1975 *Three dimensional time dependent computation of turbulent flow.* Technical Report, Stanford University.

Maxey, M. R. & Riley, J. J. 1983 Equation of motion for a small rigid sphere in a nonuniform flow. *Phys. Fluids* **26**, 883–889.

Rosales, C. & Meneveau, C. 2005 Linear forcing in numerical simulations of isotropic turbulence: Physical space implementations and convergence properties. *Phys. Fluids* **17**, 095106.

Squires, K. D. & Eaton, J. K. 1991 Preferential concentration of particles by turbulence. *Phys. Fluids* **3**, 1169–1178.

Wang, L.-P. & Maxey, M. R. 1993 Settling velocity and concentration distribution of heavy particles in homogeneous isotropic turbulence. *J. Fluid Mech* **256**, 27–68.

Zamansky, R., Coletti, F., Massot, M. & Mani, A. 2014 Radiation induces turbulence in particle-laden fluids. *Phys. Fluids* **26**, 071701.